Experimental study on hysteric behavior of composite shear walls with steel sheets

M. Hasim Kisa [a,b], S. Bahadir Yuksel [c], Naci Caglar [d,e,*]

[a] *Institute of Natural Sciences, Department of Civil Engineering, Sakarya University, Sakarya, Turkey*
[b] *Faculty of Engineering, Department of Civil Engineering, Karabuk University, Karabuk, Turkey*
[c] *Faculty of Engineering and Natural Sciences, Department of Civil Engineering, Konya Technical University, Konya, Turkey*
[d] *Faculty of Engineering, Department of Civil Engineering, Sakarya University, Sakarya, Turkey*
[e] *Faculty of Technology, Department of Civil Engineering, Sakarya University of Applied Sciences, Sakarya, Turkey*

ARTICLE INFO

ABSTRACT

Owing to demanding structural requirements, composite shear walls have become necessary in reinforced concrete high-rise structures subjected to earthquake forces. Composite shear walls also limit the inter-story drift angles during severe earthquakes in terms of their load-carrying system performance. Within the scope of this study, two types of shear walls were constructed on a 1:3 scale. One type is a conventional reinforced concrete shear wall having boundary zones consisting of only conventional reinforcement. The other walls tested were composite shear walls having boundary zones consisting of cold-formed steel sheets (CFSSs). The dimensions of the CFSSs used in the shear wall boundary zones were $2 \times L19 \times 57 \times 7$, $4 \times L23 \times 69 \times 5$, and $2 \times L17 \times 49 \times 7$ (mm). The composite shear walls were tested under cyclic lateral loadings, and their behaviors were investigated. Lateral force vs. top displacement curves with envelopes were evaluated from graphs based on the measurements, and crack propagations in the element were investigated step by step. Dissipated energy, ductility capacity, and rigidity properties based on the experimental results were compared.

1. Introduction

Reinforced concrete (RC) shear walls are used in high-rise structures that can potentially be impacted by earthquakes. The design of RC shear walls with high lateral load capacity necessitates the formation of shear wall boundary zones with narrow cross-section and intensive steel reinforcement because of the requirement for light-weight walls to reduce seismic force and the architectural goal of a smaller footprint area for a more useable floor plan. The placement of concrete for some sections with intense reinforcement is somewhat difficult and that causes application of design projects more complicated. Therefore, researchers have focused on the alternative applications of composite shear walls with ready-made profiles such as I, HSS, BOX, and TUBE sections placed at the shear wall boundary [1–6]. Researchers have also investigated different composite shear wall types with web regions having a combination of a steel plate and concrete [7–15]. In some of those studies [1,2,4], the steel profiles could not resist significant bending moments about the strong axis since they cannot reach to their section capacities, given that the steel profiles are not located at the

outermost side of the shear wall cross-section (Fig. 1(a—c)). In the other study [3], the structural steel elements are unable to restrain the bending moments and axial forces using plastic moment capacities without buckling, since the shear wall boundary steel element is not placed in a fully concrete-confined section, or slenderness effect may occur depending on the class of steel section on the steel element (Fig. 1 (d)). In other studies, the behavior of a steel shear wall supported by steel pipe filled with concrete and the effect of cold-formed steel sheets (CFSSs) on the shear walls were reported [16,17].

In this context, to obtain alternative solutions to the shortcomings of previous studies, a new type of composite shear wall was proposed with semi-compact L-shaped steel sheets instead of steel reinforcement at corners of the boundary zone of the RC shear wall. The main reason for selecting the cold-formed steel sheet (CFSS) elements is to provide easy application and placement at any side of the shear wall cross-section. This choice will also achieve the required reduction in reinforcement intensity at boundary zones of the shear wall. In addition, CFSSs can be easily formed into different thicknesses by overlapping the steel sheets. Moreover, CFSS elements can simply be applied alongside stirrups at the
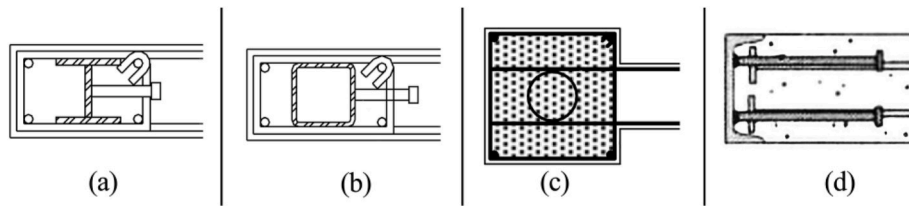
Fig. 1. Alternative applications of composite shear walls in the literature.

corners of the boundary elements thanks to their geometric compatibility providing an enhancement in load-bearing capacity of the section due to efficient confinement.

Within this scope, the boundary zones of the three composite shear walls with different configurations were constructed from the cold-formed steel sheets with L sections, and the seismic behavior of the composite shear walls was examined experimentally and compared to the conventional RC shear wall. The response of the composite shear walls was evaluated in terms of ductility, dissipated energy, and rigidity by using the displacement and load values obtained from these experiments.

2. Experimental program

To evaluate the composite shear walls with cold-formed steel sheets and conventional RC shear walls, experimental programs were conducted in the Earthquake Laboratory at the Selcuk University. Three composite shear walls with L-shaped cold-formed steel sheets were constructed and referred to as CSW-1, CSW-2, CSW-3. One conventional RC shear wall was used as a reference wall and referred to as SW in this study.

2.1. Details of shear walls

The 1:3 scaled composite shear walls were manufactured with a height, width, and length of 3300, 100, and 1000 mm, respectively (Fig. 2). The same scale factor was applied in all directions. L-section cold-formed steel sheet elements were used, and 8 mm diameter stirrups were applied at intervals of 150 mm in the composite shear wall boundary zones (Table 1). In the middle section of composite and RC shear walls, 12 rebars, 10 mm in diameter, were used (Fig. 2(b)). Sectional geometric properties of other specimens are given in Fig. 3.

Horizontal rebars were placed into the shear wall web section at

Table 1
Parameters of the SW and CSW test specimens.

Specimen label	Steel shape in boundary zone	Boundary zone steel ratio (ρ)	L_3 L_1 ⌐ $L_1/L_2/$ L_2 L_3 (mm)
SW		0.049	–
CSW-1 [18]		0.071	19/57/7
CSW-2		0.087	23/69/5
CSW-3		0.069	17/49/7

intervals of 150 mm. The slip was restricted between the surfaces of the CFSS and concrete elements by spot-welding the stirrups on the L-shaped steel elements. With this type of connection, the shear forces satisfactorily transferred without the use of headed shear stud connectors. Additionally, since the shear wall boundary zones were the focus of the study, a rigid foundation was fabricated. The foundation had dimensions of 3.00 × 0.50 × 0.70 m. The rebars were placed into the formwork parallel to the strong floor. Later, the plant-mixed concrete was casted into the formworks. Each specimen was brought to an upright position after it adequately cured. The shear wall was then anchored onto the strong ground floor at the laboratory using eight tie rods.

2.2. Material properties

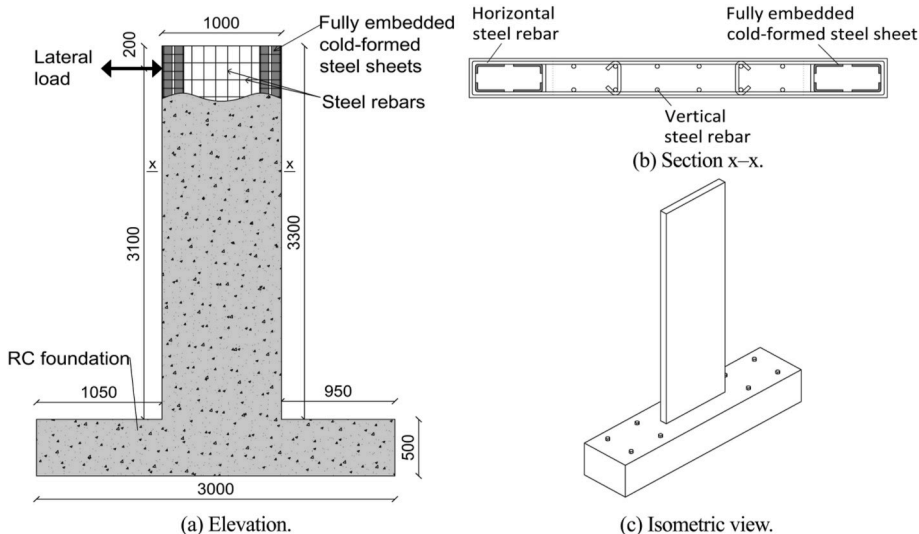Reinforcement bars of type S420 and S275JR cold-formed steel

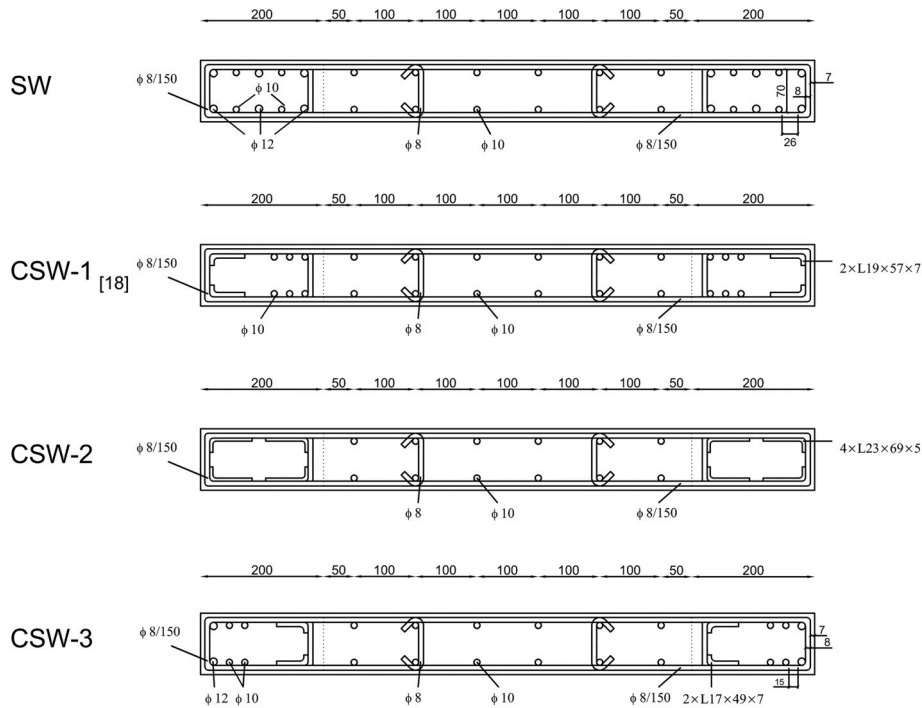**Fig. 2.** CSW-2 test specimen (units in mm).

Fig. 3. Details of the composite shear walls and conventional RC shear wall (units in mm).

sheets were used to construct the composite shear walls. The yield strength f_y and the ultimate strength f_u of steel materials were obtained by tensile tests. The elasticity moduli were observed to be approximately 210 GPa for all samples. The results related to steel properties are given in Table 2. The concrete quality used in the shear walls was a ready-mix concrete class of C25. The characteristic compressive strength f_{ck}, the mean compressive strength f_{cm}, and the secant modulus of elasticity E_{cm} of concrete specimens are presented in Table 3. The mean compressive strength f_{cm} and the secant modulus of elasticity of concrete E_{cm} were calculated from Eq. (1) and Eq. (2) according to EN 1992-1-1 [19].

$$f_{cm} = f_{ck} + 8 \tag{1}$$

$$E_{cm} = 22000(f_{cm}/10)^{0.3} \tag{2}$$

2.3. Specimen fabrication

The construction of the experimental specimen began with the preparation of CFSSs. First, the steel sheets were bent using a press machine. Next, all the steel sheets were spot-welded to each other to

obtain the different thicknesses, such that multi-layered final built-up steel sections could be created (Fig. 3). Stirrups and horizontal steel rebars were spot-welded to the CFSSs. Vertical steel elements were assembled in the reinforced concrete foundation. For anchorage, some steel elements were added to part of the vertical steel elements into the foundation. Before pouring the concrete, circular gaps were left to allow

(a) Elevation view of shear wall reinforcement.

(b) Elevation view of foundation reinforcement.

Fig. 4. Manufacturing steps for the specimens.

Table 2
Material properties of steel.

Type	Rebar diameter/Steel thickness (mm)	f_y (N/mm^2)	f_u (N/mm^2)	ε_u
Steel rebar	8	426	540.3	0.11
	10	463	565.3	0.10
	12	481	588.6	0.13
Steel sheets	2–3	270.7	351.2	0.26

Table 3
Properties of the concrete elements.

Sample no.	f_{ck} (N/mm^2)	f_{cm} (N/mm^2)	E_{cm} (N/mm^2)
1	23.5	31.5	31,040
2	24.8	32.8	31,418
3	25.4	33.4	31,590

for bolts. Subsequently, the poured concrete in formwork was vibrated then cured. After 72 h, the shear wall was removed from the formwork and positioned vertically with an overhead crane. The experimental specimens were then fixed on the strong ground with fastened bolts. The steps of the manufacturing phases are depicted in Fig. 4.

2.4. Testing methodology

Experimental specimens were tested under quasi-static cyclic loading. Tests of experimental elements were conducted on 1:3 scaled shear walls. Four specimens were evaluated under lateral loading: one

conventional RC shear wall (SW) and three composite shear walls (CSW-1 to 3). The CSW-1 specimen was tested and studied by Yüksel [18] and Yüksel and Ünal [20]. These results were compared with the results of the other specimens.

2.4.1. Test set-up

Tests were performed under reversible and increasingly lateral loads. Cyclic lateral loads were applied in the bilateral direction with specimens positioned vertically. Specimens were anchored into the strong floor with eight tie rods as shown in Fig. 5. The loading apparatus comprised a steel frame that transmitted load from a strong wall to the
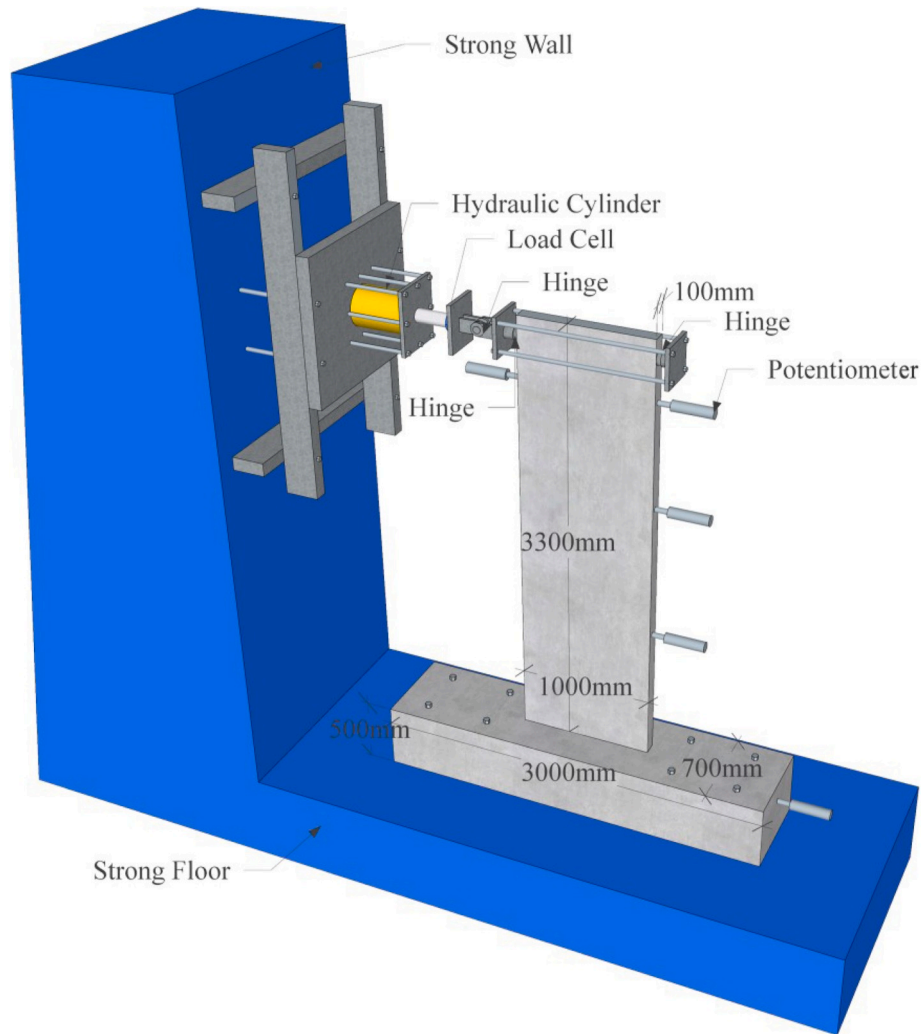
(a) Perspective view of set-up.
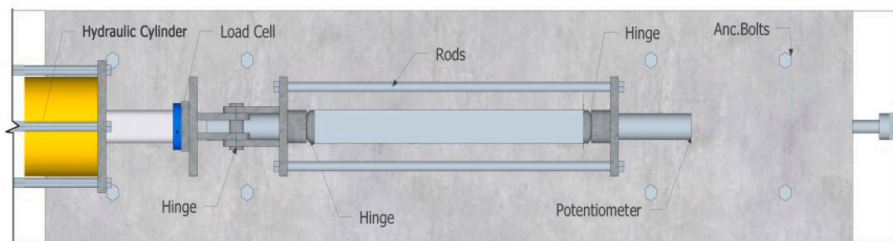
(b) Top view of set-up.

Fig. 5. Test set-up.

specimens. To obtain lateral cyclic forces, a hydraulic cylinder with a 500 kN load capacity was used.

2.4.2. Displacement history and measurements

By exerting a horizontal load with a hydraulic load transmitting apparatus connected to the hydraulic control unit in the laboratory, the tests were conducted with force-controlled and then (beyond yielding) displacement-controlled loading protocols. The displacement histories are given in Fig. 6. To gauge the range of load exerted to the composite shear walls, the data acquisition system was connected to a ~500 kN capacity load cell. The measurements were transmitted to a data processing system, which converted them to digital data by a software application. Horizontal displacement measurements were obtained using the potentiometer positioned onto the specimen at heights of 101, 203, and 283 cm (Fig. 5). To measure the undesirable slip of the foundation, measurements on the potentiometer placed at a height of 34 cm below the surface of the foundation were followed.

2.5. Experimental results

The behavior of each specimen can be characterized by four typically significant points based on the observations. These points for the conventional shear wall test specimens (SW) are shown on the lateral forces vs. top displacement skeleton curve in Fig. 7. Point 1 refers to the onset of bending cracks with the effect of cracking of concrete cover. Point 2 corresponds to the beginning of diagonal shear cracks. At Point 3, the lateral load reaches maximum capacity. Finally, the specimen loses its load-bearing capacity at Point 4 under the F_u ($\cong 0.85F_m$) loading in which F_u and F_m correspond to ultimate load and maximum load, respectively.

2.5.1. SW specimen

At the beginning of the test on the SW specimen, hairline cracks occurred in the shear wall right boundary zones under the 50 kN in the pull direction. The overlap of the cracks in the web of the shear wall was observed at a load of 70 kN in the push direction (Fig. 8(a)). At this stage, the specimen exhibited bending behavior as indicated by the horizontal crack type. The first diagonal cracks initiated when 90 kN force was reached in the push direction at a height of approximately 1.3 m (Fig. 8(b)). In this instance, the top horizontal displacement was 7.7 mm. Henceforth, the diagonal shear cracks began to propagate towards the middle section of the wall. Diagonal shear cracks in both directions completely covered the web of shear wall body until the horizontal load was reached 178.3 kN in the pull direction (Fig. 8(c)), and the top horizontal displacement was measured as 46.5 mm. At that time, the
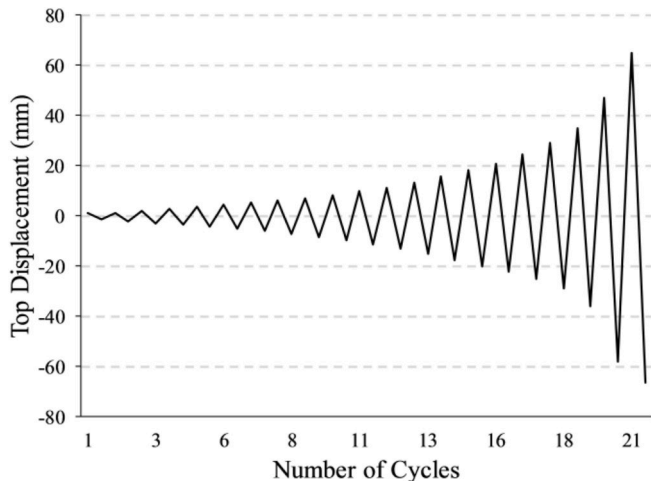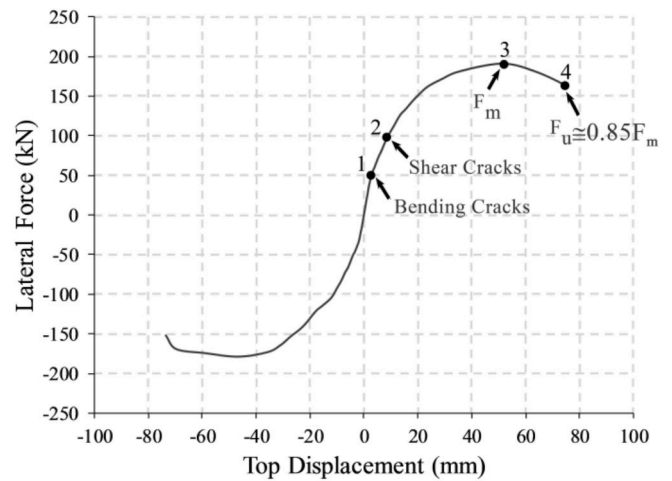

Fig. 7. Lateral force-top displacement skeleton curve for the SW specimen.

right boundary zone of the shear wall was slightly separated from the foundation. After this force point, the experiment was continued using displacement-controlled protocols, and the following target displacement was determined as 50 mm. During the later cycles, the concrete cover of the right boundary zone of the shear wall started spalling and crushing with buckling of vertical rebars while the top horizontal displacement measured 61 mm. The experiment ended when the specimen lost its load-bearing capacity reaching 102 mm displacement in the pull direction. However, only up to 85% of maximum lateral load capacities are depicted in Fig. 9. The final crack distribution of the SW specimen at the end of the loading steps is shown in Fig. 8(d).

2.5.2. CSW-2 specimen

In the force-controlled part of the test for the CSW-2 specimen, small cracks spreading up to a height of 1.5 m were measured in the shear wall boundary zones when a force of 50 kN was attained in both directions. A hairline crack, similar to the bending fracture line, appeared in both the foundation and the web section on the composite shear wall with a 60 kN force in the pull direction (Fig. 10(a)). These crack lines parallel to the horizontal plane revealed the ductile behavior of the structure at small displacement ranges. In this situation, the top horizontal displacement was approximately 5 mm. The formation of cracks in the boundary zones of CSW-2 showed that shear wall stresses intensified in the boundary zone. Diagonal shear cracks became apparent under 110 kN load in the pull direction at a height of 100 cm, and the top horizontal displacement was gauged as 11 mm (Fig. 10(b)). Under a 120 kN load, a secondary crack formed in the opposite direction to the diagonal crack occurred in the previous cycle. After this stage, the bending behavior of the shear wall interchanged step by step into a shear behavior. In the ongoing cycles, the specimen was translated by 28 mm under a 180 kN load in the pull direction. The loss of strength in the pressure partition at the conjunction between the shear wall and the foundation block, as well as the crack range in the tensile zone, remained even. The shear wall was translated by 47 mm under a 200 kN load in the push direction. The maximum force level occurred at approximately 200.7 kN in the pull direction and caused a 57.9 mm displacement (Fig. 10(c)). However, the CFSSs became visible when the concrete covers spalled in both boundary zones. After this force point, cracks tended to widen rather than propagate. Since the force on the specimen could not be applied any further beyond this level, the experiment was continued with the displacement-controlled protocol. Buckling occurred in the CFSSs at the right end of the composite shear wall once the specimen could not carry any further loading causing a target displacement of 66.9 mm in the pull direction. The experiment was terminated when the steel element at the left end of the shear wall lost the load-bearing capacity after it was completely buckled just below the welding that connecting the plates.
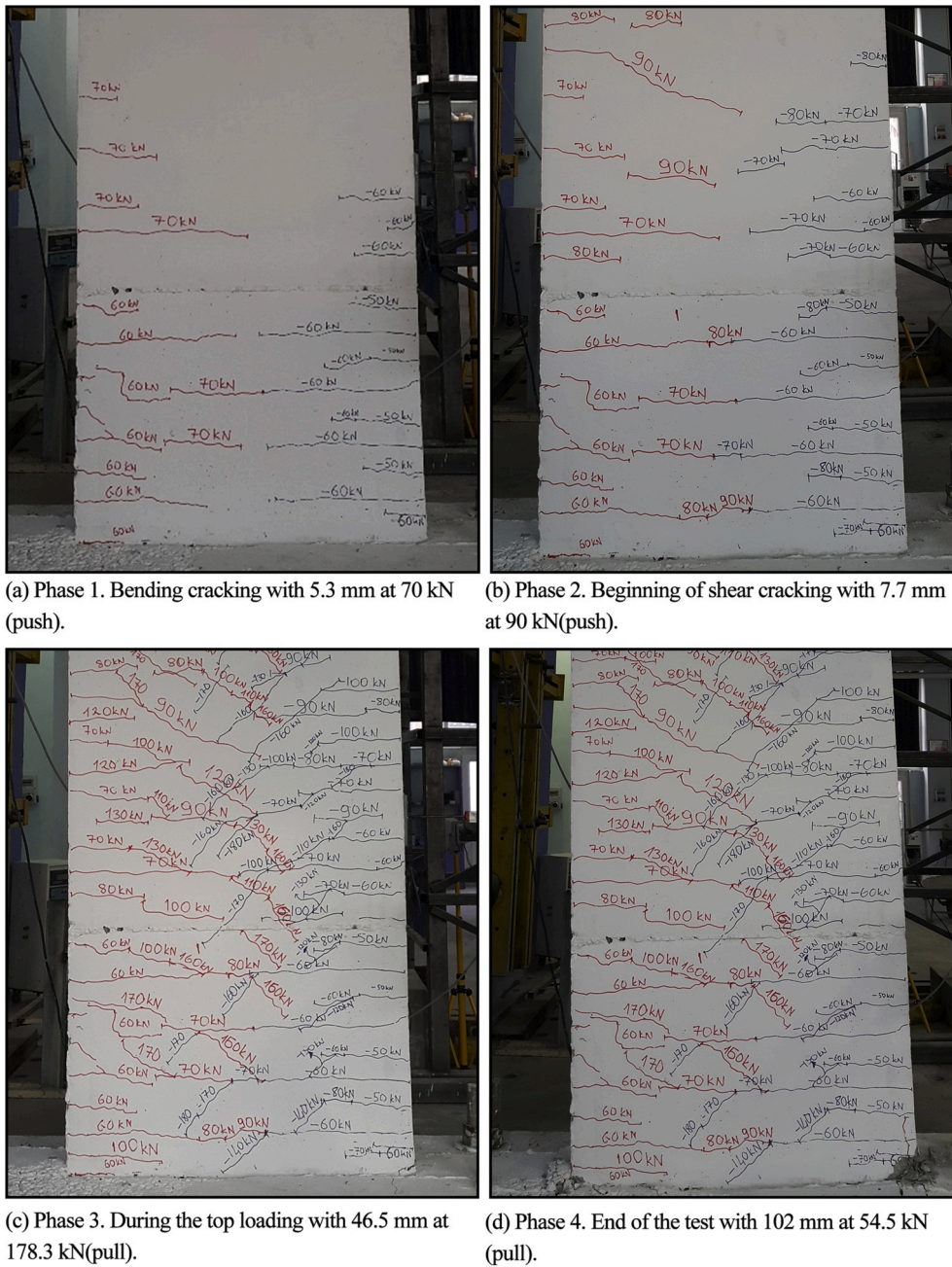

Fig. 6. Displacement history.

(a) Phase 1. Bending cracking with 5.3 mm at 70 kN (push).

(b) Phase 2. Beginning of shear cracking with 7.7 mm at 90 kN(push).

(c) Phase 3. During the top loading with 46.5 mm at 178.3 kN(pull).

(d) Phase 4. End of the test with 102 mm at 54.5 kN (pull).

Fig. 8. General failure behavior for the SW specimen.

The final fracture distribution of the test specimen at the end of the loading steps is shown in Fig. 10(d). The graph of the lateral force vs. top displacement curve obtained based on the measurements at the top is given in Fig. 11.

2.5.3. CSW-3 specimen

In the CSW-3 specimen, 2×L17×49×7 CFSSs were used in each boundary zone, unlike the SW specimen. The test specimen was formed by positioning the CFSS in the boundary zone of the CSW-1 specimen near the web section. The rest of the reinforcement distribution was similar to the SW specimen except for the boundary zones. In the force-controlled part of the test, small cracks spreading up to a height of 1.5 m appeared in the shear wall boundary zones when a force of 60 kN was attained in both directions. At the load level of 60 kN in both directions, a hairline crack formed at the conjunction of the foundation block and

the shear wall, similar to a bending crack type (Fig. 12(a)). In this case, the top displacement was measured at 4.2 mm. Under a load of 100 kN in the push direction, the cracks merged owing to the pulling and pushing forces. Instead of bending behavior in the shear wall, shear behavior began to dominate (Fig. 12(b)). The top displacement was measured as 8.5 mm. During the 170 kN loading in the push direction, the first crushes in the pressure zone were observed when displacement reached 23 mm. An increase in the crush on the right end occurred at a load level of 203.4 kN in the push direction (Fig. 12(c)). The top displacement was measured as 52.3 mm. After this stage, the experiment was conducted with displacement control. Rebar buckling formed at the right boundary zone with 65 mm of displacement in the push direction. The test was terminated when the specimen reached 68.5 mm in displacement (Fig. 12(d)). The lateral force vs. top displacement curve obtained based on the measurements at the top of the specimen is given in Fig. 13.
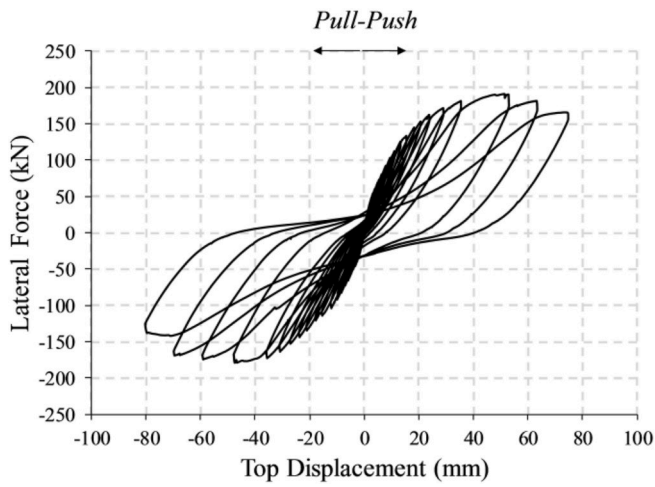
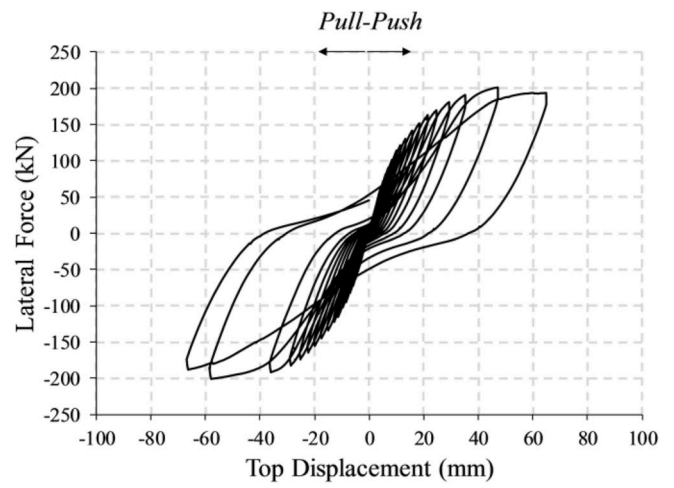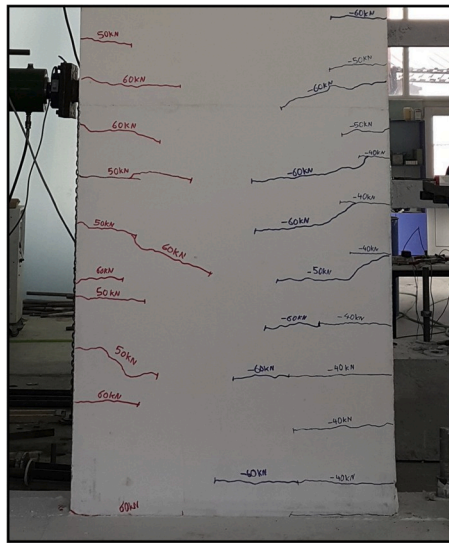**Fig. 9.** Lateral force-top displacement curve for the SW specimen.
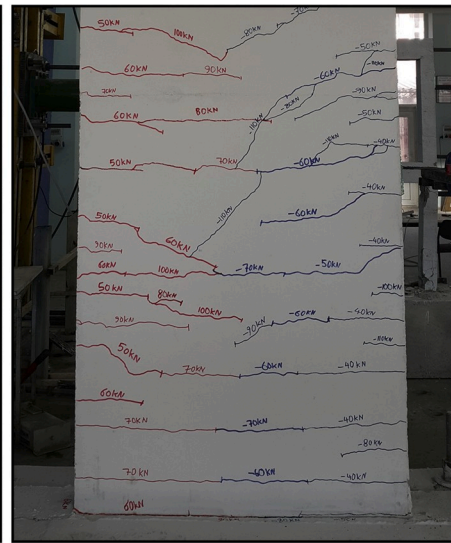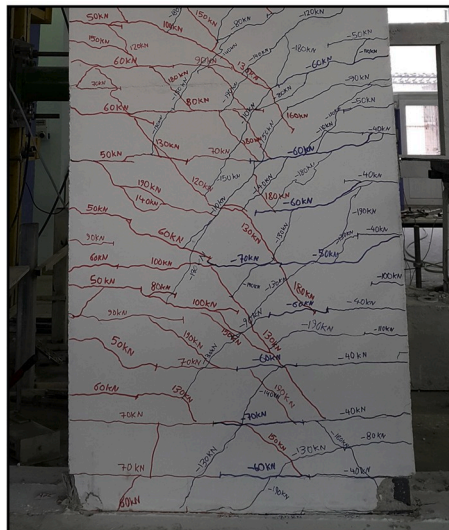

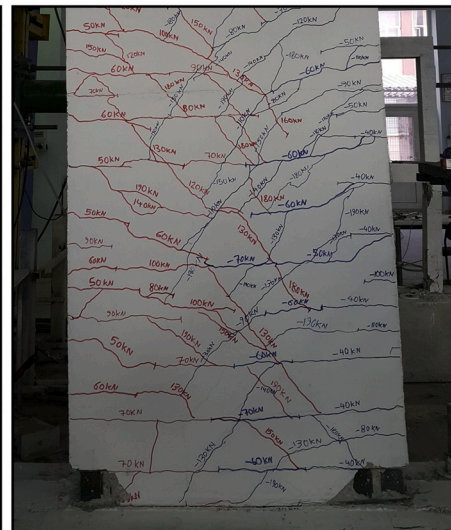**Fig. 11.** Lateral force-top displacement curve for the CSW-2 specimen.

(a) Phase 1. Bending cracking with 5 mm at 60 kN (pull).

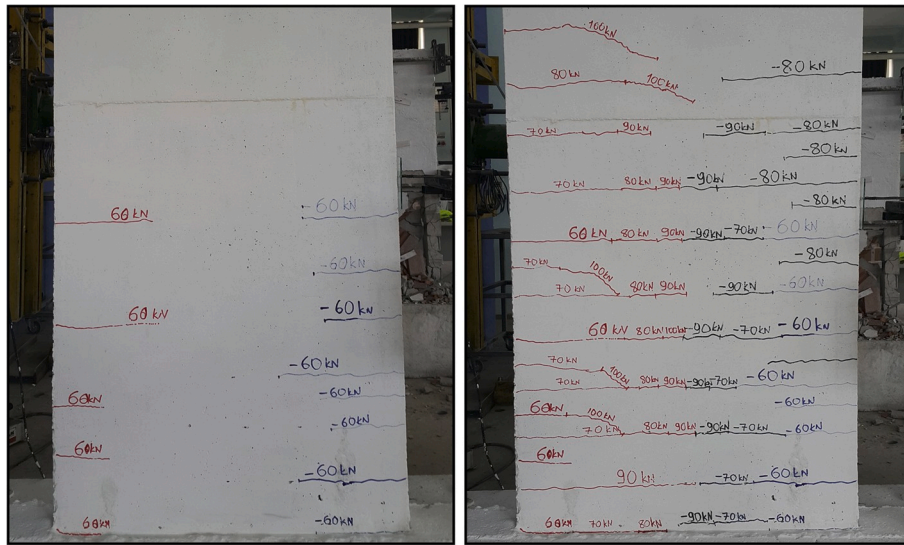(b) Phase 2. Beginning of shear cracking with 11 mm at 110 kN(pull).

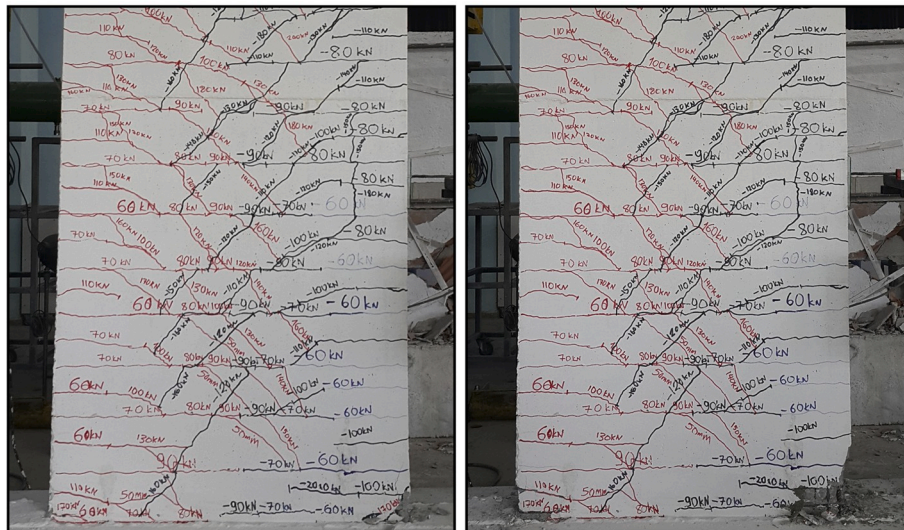(c) Phase 3. During the top loading with 57.9 mm at 200.7 kN(pull).

(d) Phase 4. End of the test with 66.9 mm at 173.9 kN (pull).

Fig. 10. General failure behavior for the CSW-2 specimen.

(a) Phase 1. Bending cracking with 4.2 mm at 60 kN (pull).

(b) Phase 2. Beginning of shear cracking with 8.5 mm at 100 kN(push).

(c) Phase 3. During the top loading with 52.3 mm at 203.4 kN(push).

(d) Phase 4. End of the test with 68.5 mm at 175.3 kN (push).

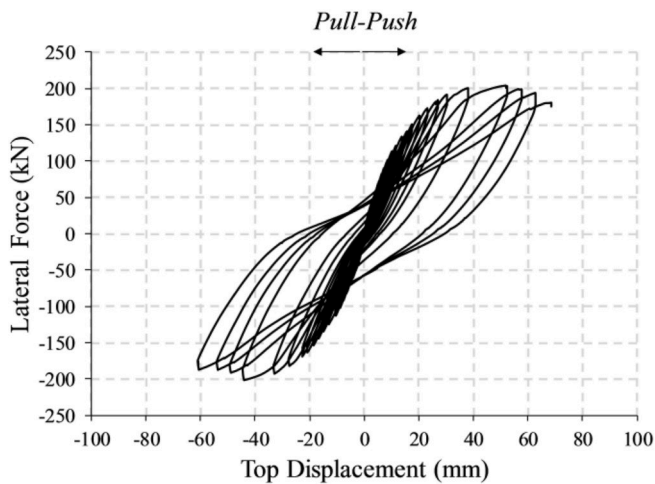**Fig. 12.** General failure behavior for the CSW-3 specimen.

Fig. 13. Lateral force-top displacement curve for the CSW-3 specimen.
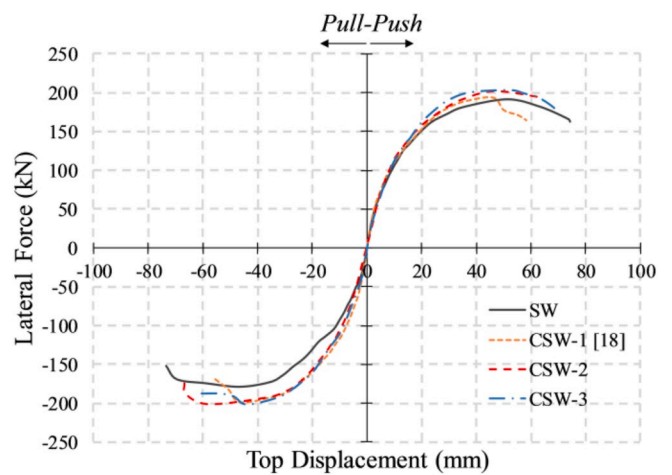

Fig. 14. Comparative lateral force-top displacement curves.

3. Comparative study

The lateral force vs. top displacement skeleton curves for all specimens were generated by connecting the peak points on hysteretic loading steps and are presented in Fig. 14.

The upper limit of lateral force achieved by the CSW-3 specimen was 7% higher than the conventional RC shear wall (SW) in the push direction. In the pull direction, the CSW-3 specimen displayed a lateral load-bearing capacity 12% higher than that of the SW specimen. The CSW-1 specimen failed at the lower displacement level compared to the other specimens. Because of the testing protocols, similar envelope curves were obtained under the hysteretic loading. The failure modes of specimens' boundary zones are given in Fig. 15.

3.1. Displacement ductility

The ductility of the composite shear wall is a significant characteristic that indicates the displacement capacity after yielding point. The displacement ductility ratio is determined by dividing the ultimate displacement Δ_u by the yielding displacement Δ_y. The yield displacement was established based on the method shown in Fig. 16 [21], in which the yield displacement is equivalent to the abscissa at the yielding stage on the curve. This value is found at the intersection point between the horizontal line at F_{max} and the connecting line between 75% of F_{max} and the origin point. The horizontal displacement at the point when the maximum horizontal force drops 15% is called the ultimate displacement Δ_u. Although all specimens were loaded up to maximum carrying load capacity during the test, only up to 85% of maximum lateral load capacities are presented for the skeleton curves in Fig. 14 according to
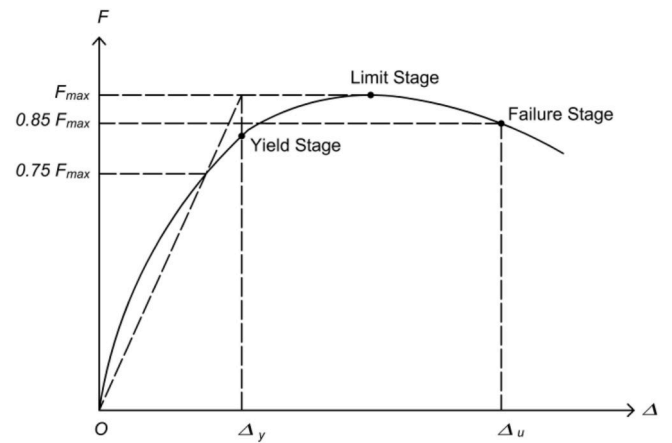

Fig. 16. Determination of yielding and failure stage [21].

the Δ_u definition. The significant points of the lateral force vs. top displacement skeleton curves are given in Table 4. Displacement ductility ratios for each tested specimen are shown comparatively in Fig. 17. The CSW-3 specimen exhibited higher ductile behavior than the other CSW specimens.

3.2. Dissipated energy

The dissipation of energy was determined from the area under envelopes of the lateral force vs. top displacement curves. The calculated dissipated energy values for each specimen are compared in Fig. 18. The CSW-2 and CSW-3 specimens exhibited better behavior than the conventional RC shear wall in terms of dissipated energy, while the CSW-1 dissipated energy values were smaller than that of the conventional RC shear wall.

3.3. Stiffness degradation

The rigidity of the specimens, shown in Fig. 19, is a function of the average secant stiffness at different displacement levels. The formula of average secant stiffness is given in Eq. (3) [22]:

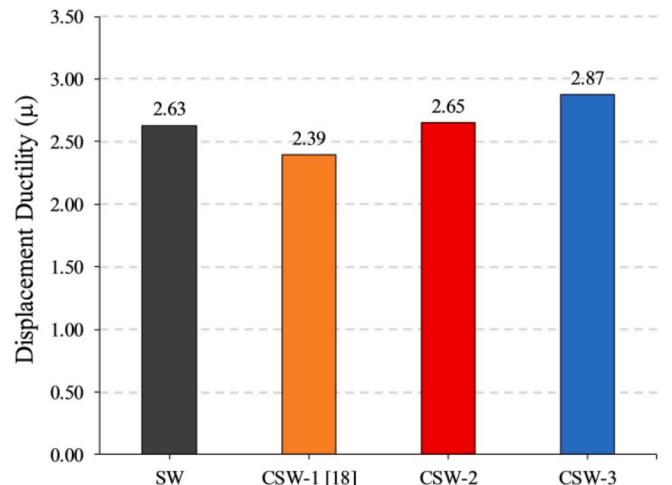$$K_i = \frac{P_i^{(+)} - P_i^{(-)}}{\Delta_i^{(+)} - \Delta_i^{(-)}} \tag{3}$$

(a) SW-left boundary zone. (b) SW-right boundary zone.

(c) CSW-2-left boundary zone. (d) CSW-2-right boundary zone.

(e) CSW-3-left boundary zone. (f) CSW-3-right boundary zone.

Fig. 15. The failure modes of steel elements.

Fig. 17. Comparative displacement ductility (μ).

Table 4
Force and displacement at different characteristic points.

Point specimen	Yield stage		Limit stage		Failure stage	
	P_y (kN)	Δ_y (mm)	P_{max} (kN)	Δ_{max} (mm)	$P_{85\%}$ ($\cong$) (kN)	Δ_u (mm)
SW	−154.73	−27.90	−178.371	−46.518	−151.615	−73.37
CSW-1 [18]	−141.79	−23.13	−198.050	−46.242	−168.343	−55.34
CSW-2	−170.87	−25.27	−200.722	−57.926	−173.991	−66.93
CSW-3	175.80	23.84	203.436	52.328	175.314	68.52

in which $P_i^{(+)}$ and $P_i^{(-)}$ correspond to extremum lateral load at positive and negative directions per number of cycles for each loading, respectively, where $\Delta_i^{(+)}$ and $\Delta_i^{(-)}$ represent the extremum lateral displacement points.

As a result of initial loading stages, the stiffness degradation shows similar characteristics for all specimens. Initial rigidity capacities of the composite shear wall specimens were found to be between 13.2 and 15.2 kN/mm at a 5 mm displacement point. Compared to the conventional shear wall, the CSW-1 specimen exhibited the highest rigid behavior (Fig. 19).
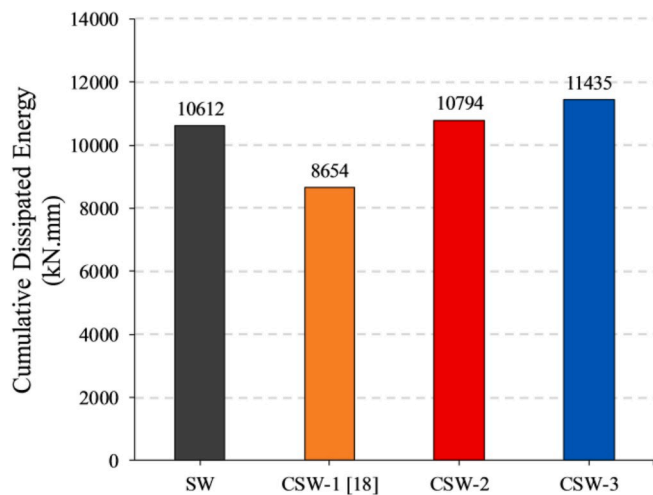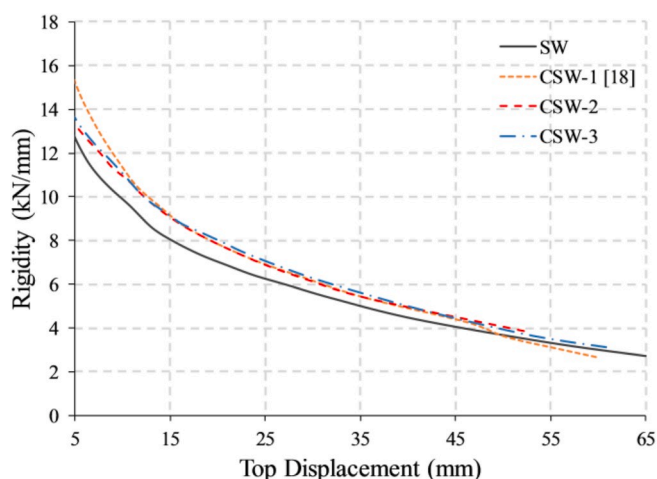

Fig. 18. Comparative cumulative dissipated energy.

Fig. 19. Stiffness degradation vs. top displacement.

4. Conclusions

This study experimentally analyzes the behavior of composite shear walls with L-shaped vertical steel sheets compared to conventional shear walls. The encastered specimens at 1:3 scales were subjected to cyclic lateral loading. The effects of different configurations of CFSS on the total response were evaluated in terms of ductility, dissipated energy, and rigidity. Some conclusions have been established within the restriction of the tested specimens:

- Composite shear walls with L-shaped cold-formed steel sheets had lateral load capacities ranging from 11% to 14% more than the conventional RC shear wall. All the specimens exhibited flexural behavior during the failing stages. Failing initiated with the crushing of concrete cover on the compression zone of the shear wall. After the crushing of concrete, lateral capacity dropped owing to the buckling of vertical steel sheets.
- Local buckling of the CFSSs first occurred in the CSW-1 specimen at the compression zone, while the buckling started at higher displacement levels for the CSW-2 and CSW-3 specimens. Since the steel elements have a high tendency for buckling, placing CFSS elements near the web region in the boundary zone helps to consume more energy and avoid buckling.
- The dissipated energy capacity of the CSW-3 specimen was found to be higher by 6% than the CSW-2, which had a higher capacity than the SW specimen by 2%. Moreover, the dissipated energy capacity of the SW specimen was higher than the CSW-1 specimen by 23%. High ductility capacity was exhibited by the CSW-3 configuration owing to its higher dissipated energy.
- The CSW-1 specimen demonstrated stiffer behavior at initial stages indicating the contribution of L-shaped steel elements on rigidity. Additionally, all the composite specimens had approximately 12% higher rigidity value more than the conventional shear wall specimen between an inter-story drift angle of 0.004 and 0.015 rad. However, the local buckling problem of the CSW-1 and CSW-2 specimens could have been improved by increasing sheet thickness.
- Placing cold-formed steel sheets on the outer side of boundary regions could effectively improve the flexural capacity of a shear wall. However, according to the results of the study, this would depend not only on the configurations of CFSSs but also on their cross-section slenderness ratio.

Declaration of competing interest

The authors declare that they have no known competing financial interests or personal relationships that could have appeared to influence the work reported in this paper.

CRediT authorship contribution statement

M. Hasim Kisa: Methodology, Formal analysis, Investigation, Writing - original draft, Writing - review & editing. **S. Bahadir Yuksel:** Conceptualization, Methodology, Investigation, Resources, Writing - review & editing. **Naci Caglar:** Methodology, Investigation, Writing -

review & editing.

References

[1] D. Dan, A. Fabian, V. Stoian, Theoretical and experimental study on composite steel–concrete shear walls with vertical steel encased profiles, J. Constr. Steel Res. 67 (2011) 800–813, https://doi.org/10.1016/j.jcsr.2010.12.013.

[2] D. Dan, A. Fabian, V. Stoian, Nonlinear behavior of composite shear walls with vertical steel encased profiles, Eng. Struct. 33 (2011) 2794–2804, https://doi.org/10.1016/j.engstruct.2011.06.004.

[3] S.H. Cho, B. Tupper, W.D. Cook, D. Mitchell, Structural steel boundary elements for ductile concrete walls, J. Struct. Eng. 130 (2004) 762–768, https://doi.org/10.1061/(ASCE)0733-9445(2004)130:5(762).

[4] J. Qian, Z. Jiang, X. Ji, Behavior of steel tube-reinforced concrete composite walls subjected to high axial force and cyclic loading, Eng. Struct. 36 (2012) 173–184, https://doi.org/10.1016/j.engstruct.2011.10.026.

[5] F.Y. Liao, L.H. Han, Z. Tao, Performance of reinforced concrete shear walls with steel reinforced concrete boundary columns, Eng. Struct. 44 (2012) 186–209, https://doi.org/10.1016/j.engstruct.2012.05.037.

[6] F.-Y. Liao, L.-H. Han, Z. Tao, Seismic behaviour of circular CFST columns and RC shear wall mixed structures: Experiments, J. Constr. Steel Res. 65 (2009) 1582–1596, https://doi.org/10.1016/j.jcsr.2009.04.023.

[7] Q. Zhao, A. Astaneh-Asl, Cyclic behavior of traditional and innovative composite shear walls, J. Struct. Eng. 130 (2004) 271–284, https://doi.org/10.1061/(ASCE)0733-9445(2004)130:2(271).

[8] S. Dey, A.K. Bhowmick, Seismic performance of composite plate shear walls, Structure 6 (2016) 59–72, https://doi.org/10.1016/j.istruc.2016.01.006.

[9] L. Shahryari, M. Esfandiari, Comparison of plasticity and stiffness of steel shear walls with composite steel plate shear wall, J. Struct. Eng. Geotech. 5 (2015) 21–26.

[10] M. Meghdadaian, M. Ghalehnovi, Improving seismic performance of composite steel plate shear walls containing openings, J. Build. Eng. 21 (2019) 336–342, https://doi.org/10.1016/j.jobe.2018.11.001.

[11] M. Meghdadian, N. Gharaei-Moghaddam, A. Arabshahi, N. Mahdavi, M. Ghalehnovi, Proposition of an equivalent reduced thickness for composite steel plate shear walls containing an opening, J. Constr. Steel Res. 168 (2020), https://doi.org/10.1016/j.jcsr.2020.105985.

[12] H.-S. Hu, J.-G. Nie, J.-S. Fan, M.-X. Tao, Y.-H. Wang, S.-Y. Li, Seismic behavior of CFST-enhanced steel plate-reinforced concrete shear walls, J. Constr. Steel Res. 119 (2016) 176–189, https://doi.org/10.1016/j.jcsr.2015.12.010.

[13] N.H. Nguyen, A.S. Whittaker, Numerical modelling of steel-plate concrete composite shear walls, Eng. Struct. 150 (2017) 1–11, https://doi.org/10.1016/j.engstruct.2017.06.030.

[14] Q.Q. Liang, B. Uy, H.D. Wright, M.A. Bradford, Local and post-local buckling of double skin composite panels, Proc. Inst. Civ. Eng. - Struct. Build. 156 (2003) 111–119, https://doi.org/10.1680/stbu.2003.156.2.111.

[15] S. Epackachi, A.S. Whittaker, A. Aref, Seismic analysis and design of steel-plate concrete composite shear wall piers, Eng. Struct. 133 (2017) 105–123, https://doi.org/10.1016/j.engstruct.2016.12.024.

[16] A. Astaneh-Asl, Q. Zhao, Cyclic Tests of Steel Shear Walls, 2002, https://doi.org/10.13140/RG.2.2.19642.85443. Berkeley.

[17] M.H. Kısa, S.B. Yüksel, N. Çağlar, An experimental study on the hysteric behavior of composite shear walls, in: 4th Int. Symp. Innov. Technol. Eng. Sci, ISITES2016, 2016, pp. 1574–1582.

[18] S.B. Yüksel, Seismic Behaviour of Composite Shear Walls Having L Shaped Steel Profiles as Longitudinal Boundary Reinforcement, Selçuk University, Scientific Research Project (SU BAP), 2016. Project number: 14101011.

[19] EN 1992-1-1 (2004), Eurocode 2: Design of Concrete Structures - Part 1-1: General Rules and Rules for Buildings, 2004.

[20] S.B. Yüksel, A. Ünal, Experimental behavior of composite shear walls having L shape steel sections in boundary regions, in: World Acad. Sci. Eng. Technol. Int. J. Civil, Environ. Struct. Constr. Archit. Eng, 2015, https://doi.org/10.5281/zenodo.1108058.

[21] H. Zhang, J. Dong, Y. Duan, X. Lu, J. Peng, Seismic and power generation performance of U-shaped steel connected PV-shear wall under lateral cyclic loading, Int. J. Photoenergy (2014) 1–15, https://doi.org/10.1155/2014/362638, 2014.

[22] J. Wang, Z. Wang, Y. Tang, T. Liu, J. Zhang, Cyclic loading test of self-centering precast segmental unbonded posttensioned UHPFRC bridge columns, Bull. Earthq. Eng. 16 (2018) 5227–5255, https://doi.org/10.1007/s10518-018-0331-y.